NANO LETTERS

Letter

pubs.acs.org/NanoLett

A Sugar-Derived Room-Temperature Sodium Sulfur Battery with Long Term Cycling Stability

Rachel Carter,[†] Landon Oakes,[†,‡] Anna Douglas,[†,‡] Nitin Muralidharan,[†,‡] Adam P. Cohn,[†] and Cary L. Pint*[,†,‡]

[†]Department of Mechanical Engineering and [‡]Interdisciplinary Materials Science Program, Vanderbilt University, Nashville, Tennessee 37235, United States

Supporting Information

ABSTRACT: We demonstrate a room-temperature sodium sulfur battery based on a confining microporous carbon template derived from sucrose that delivers a reversible capacity over 700 mAh/g_S at 0.1C rates, maintaining 370 mAh/g_S at 10 times higher rates of 1C. Cycling at 1C rates reveals retention of over 300 mAh/g_S capacity across 1500 cycles with Coulombic efficiency >98% due to microporous sulfur confinement and stability of the sodium metal anode in a glyme-based electrolyte. We show sucrose to be an ideal platform to develop microporous carbon capable of mitigating electrode−electrolyte reactivity and loss of soluble intermediate discharge products. In a manner parallel to the low-cost materials of the traditional sodium beta battery, our work demonstrates the combination of table sugar, sulfur, and sodium, all of which are cheap and earth abundant, for a high-performance stable room-temperature sodium sulfur battery.

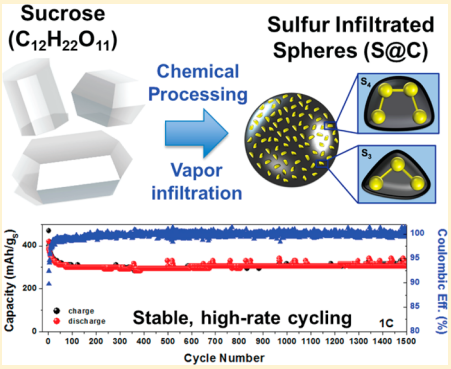

KEYWORDS: *Sodium sulfur battery, sulfur confinement, microporous carbon, sucrose-derived carbon, room temperature, ambient temperature*

The sodium beta battery was developed in the 1960s by Ford Motor Company under the promise that it could deliver the cost and performance metrics required for battery-powered electric vehicles.[1] This battery design involves a sodium anode, a sulfur cathode, a beta-alumina solid separator, and operation at temperatures >300 °C. The high temperature enables sodium wetting on the beta alumina, diffusion of sodium ions to the cathode, and the molten cathode to sustain a soluble media for sodium polysulfide species. Despite the loss of interest in electric vehicles in the mid-19th century, the sodium-beta battery emerged as a staple low-cost battery system that remains commercially available today and routinely used for commercial load-leveling applications.[2] However, despite its excellent material cost/performance ratio,[3] the high operation temperature prohibits its practicality in applications that currently command the rechargeable battery market and operate at room temperature, leaving these systems only useful for niche applications.[4] Nonetheless, the capability to design a battery with the cost/performance metrics of a sodium beta battery but with stable room-temperature operation could be disruptive to current battery-powered technologies[3] and specifically provide a practical path toward stationary grid storage with lifetime energy cost below 1 ¢/kWh. Compared to battery markets for portable electronics or mobile systems where gravimetric performance and safety dictate feasibility over other metrics, batteries for residential or commercial stationary storage require low-cost, long lifetime, and good rate accessibility to yield lifetime cost-per-unit-energy of <∼0.12 ¢/kWh after coupling with an energy generation source, such as photovoltaic cells, requiring a battery cost <0.01−0.02 ¢/kWh in (optimistic) current market conditions. Unlike current lithium-ion batteries, room-temperature sodium−sulfur batteries give promise for stationary units displaying all of these metrics and exhibiting energy density comparable to or better than current lithium-ion batteries.

In recent years, the protégé for room-temperature sodium sulfur batteries, lithium−sulfur batteries, have emerged as an appealing replacement for current lithium-ion batteries boasting a two-electron transfer per sulfur atom, delivering 6 times the energy density of Li-ion, and overcoming cost and safety issues of conventional cobalt-containing cathodes. As significant research has addressed key issues such as polysulfide shuttling that limits cycling stability, continued challenges remain, including anode stability that must be addressed with consumable lithium nitrate additives,[5] and routes that can intersect conventional battery manufacturing facilities and enable high areal loadings.[6] Whereas bottlenecks remain to reach a battery with 500 Wh/kg energy density, a critical goal of Li−S battery technology, in this work we highlight that the rational design of a sodium−sulfur battery with a competitive energy density to Li-ion batteries can overcome current bottlenecks challenging Li−S batteries, enabling a key platform

Received: December 13, 2016
Revised: January 24, 2017
Published: February 2, 2017

DOI: 10.1021/acs.nanolett.6b05172
Nano Lett. 2017, 17, 1863−1869

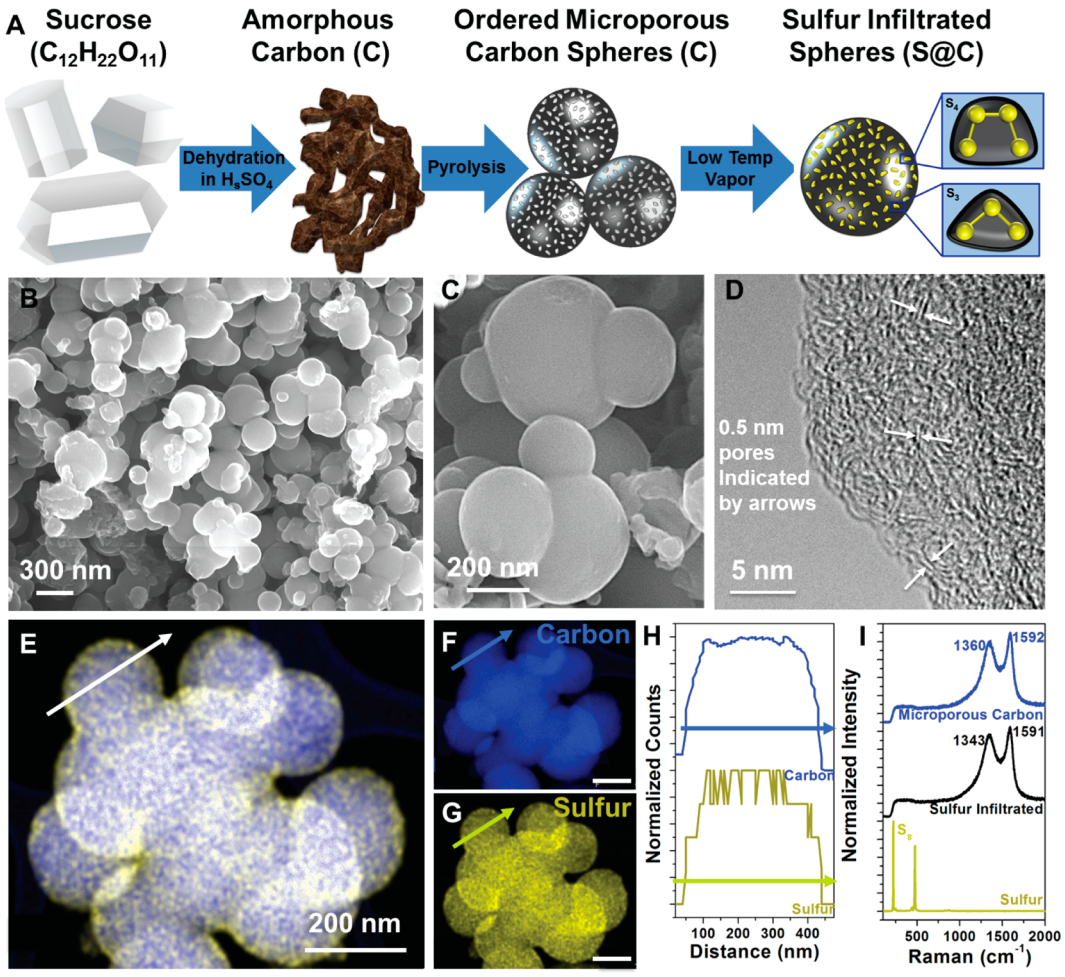

Figure 1. (A) Schematic representation of the material processing steps of using sucrose (sugar) to produce microporous sodium sulfur battery cathodes. Scanning electron microscope image of microporous carbon with spheres at (B) low and (C) higher magnification. (D) TEM image showing morphology of micropores inside the carbon spheres, (E) STEM EDS composite map with carbon (blue) and sulfur (yellow). (F,G) Individual element maps and (H) linescan across the diameter of a microporous carbon sphere infiltrated with sulfur. (I) Raman spectroscopy of microporous carbon sulfur infiltrated spheres and as received sulfur powder.

for future grid scale stationary storage units where cost trumps energy density in market feasibility. The similar discharge mechanisms of the alkali metals involve incremental discharge from elemental sulfur (stored as S_8 molecules) through intermediate products (M_2S_8, M_2S_6, M_2S_4; M = Li or Na), which are soluble in the commonly used organic electrolytes, to the final products M_2S_2 and M_2S, which are insoluble.[4,6,7] Particular challenges with room-temperature sodium sulfur batteries compared to lithium sulfur batteries are the greater volume expansion (260% for Na versus 80% for Li),[4] low-measured Coulombic efficiencies due to instability at both the anode and cathode,[7−11] and poor understanding of soluble discharge products.[7] Additionally, whereas manufacturing costs must be minimized in stationary cells, functional electrode materials must involve cheap, if any, processing and from bulk forms of sodium, sulfur, and/or carbon.

One emerging strategy for mitigating soluble products in lithium−sulfur batteries is by microporous confinement, where all sulfur is stored in the system as molecules limited to the sizes S_{2-4}, where S_4 is the largest sulfur molecule permitted in the material interior, by controlling the size of pores in the host. Confinement efforts for lithium sulfur batteries were abandoned because the necessary micropore size (<1 nm) limits sulfur mass loadings to under 50 wt %,[12−16] and higher loadings (>70%) are necessary to reach appropriately high gravimetric energy density that dictates their use as advanced Li-ion carriers.[6] However, early sodium sulfur batteries without confinement (elemental S_8 cathodes) yield poor sulfur conversion[8,11,17−21] unless additional device elements including interlayers or dense solid electrolytes adding excessive mass, volume, and cost are employed.[9,10,22−24] Whereas microporous confinement lowers the overall energy density because higher voltage conversion of soluble products is excluded, effective implementation of the strategy can still deliver 2 times the energy density of Li-ion and significant reliability is gained.[4] Initial confinement works have shown significantly improved sulfur conversion and cyclability[25−31] (Table S1) but all suffer from low Coulombic efficiency due to an unstable anode-electrolyte interface.

In this work, we realize this promising approach by demonstrating a microporous confinement cathode for a room-temperature sodium sulfur battery based on processing store-bought table sugar and infiltrating sulfur into micropores using scalable isothermal vapor phase infiltration. The confinement strategy mitigates polysulfide shuttling at the cathode and is assembled with a glyme-based electrolyte, which provides a

DOI: 10.1021/acs.nanolett.6b05172
Nano Lett. 2017, 17, 1863−1869

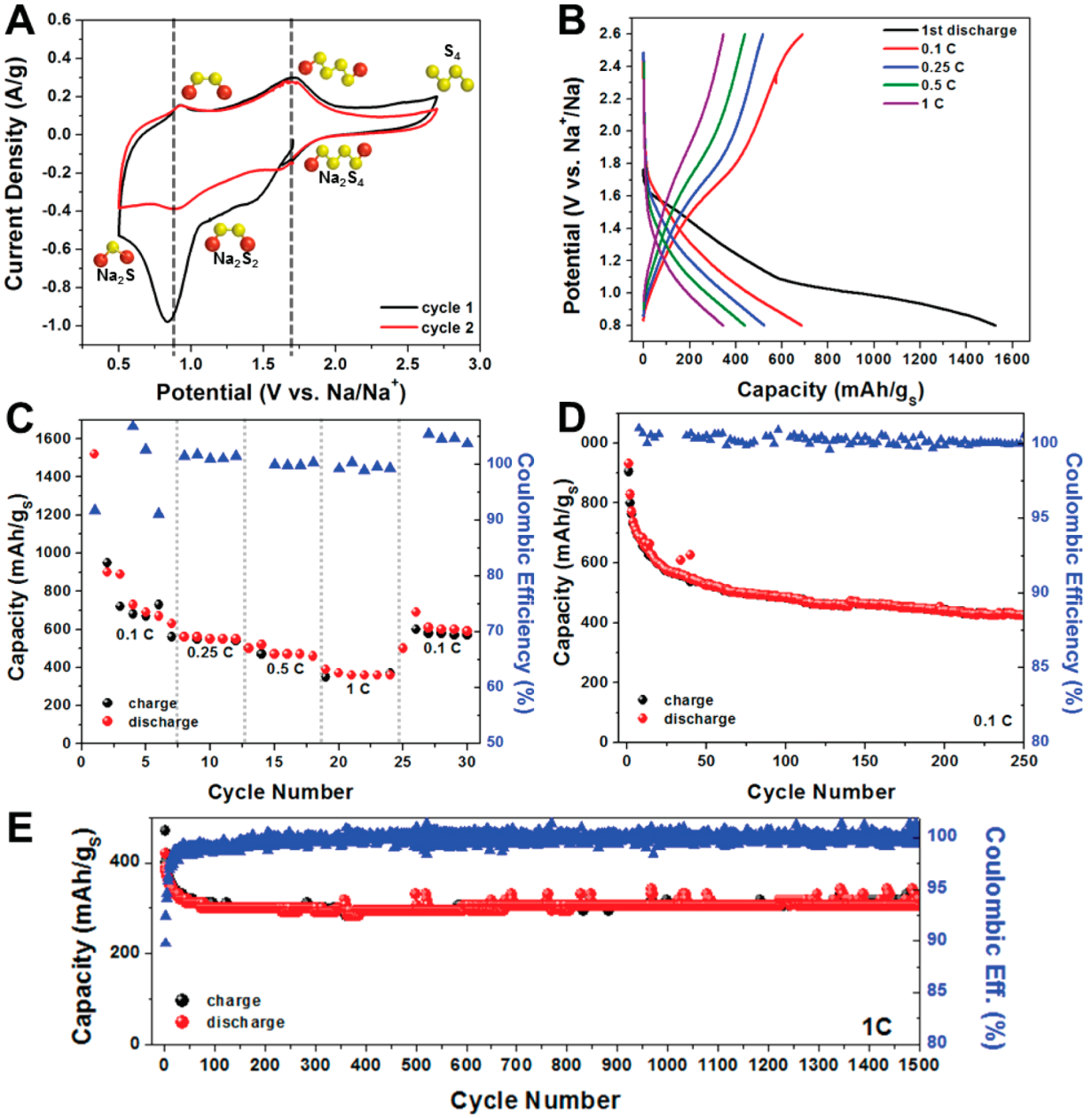

Figure 2. (A) Cyclic voltammetry of sulfur cathode at 50 μV/s with sodium/sulfur interactions pictorially represented, (B) galvanostatic charge/discharge profiles at various charging rates, (C) capacity and Coulombic efficiency with >5 cycles at each rate, (D) 250 cycles at 0.1C with discharge and charge capacity plotted at each cycle and Coulombic efficiency plotted as blue triangles with axis at the right, and (E) 1500 cycles at 1C in same format as panel D.

stable sodium-electrolyte interface[32] that overcomes low Coulombic efficiency. The stability of both electrodes delivers significantly enhanced Coulombic efficiency (>98%) over previous works on Na−S batteries (50−80%).[4,7] We demonstrate a platform that exhibits exceptional durability over 1500 cycles while still delivering above 300 mAh/g_S at high rates of 1C.

To realize a microporous sulfur-confining host, we processed table sugar into microporous carbon−sulfur composite materials. Here, as received sugar ($C_{12}H_{22}O_{11}$) was controllably dehydrated in a 5 M solution of sulfuric acid at 120 °C for 10 h to leave behind only amorphous carbon (Figure 1A). This process controllably utilizes the violent exothermic reaction between pure sulfuric acid and sugar for higher precision at the nanoscale. The rinsed amorphous carbon precipitate was pyrolized under low pressure Ar flow for 2 h at 850 °C[33,34] leaving carbon spheres of ranging diameter (50−500 nm) seen in Figure 1B,C containing micropores (Figure 1D) with size of ∼0.5 nm, verified through fast Fourier transform (FFT) analysis of transmission electron microscopy (TEM) images (Figure S4) and agreeing well with other reports of sugar-derived microporous carbons.[14,33,34] Some more visually apparent pores of size agreeing with FFT are indicated with double arrows in Figure 1D. Finally, the prepared carbon powder is infiltrated with sulfur by low temperature (175 °C) isothermal vapor phase process[35] lasting 1 h and resulting in 35 wt % sulfur completely confined in the micropores of the carbon spheres. Whereas this is a lower mass ratio of sulfur than that required for high energy lithium−sulfur batteries, the cathode stability enabled by microporous confinement

DOI: 10.1021/acs.nanolett.6b05172
Nano Lett. 2017, 17, 1863−1869

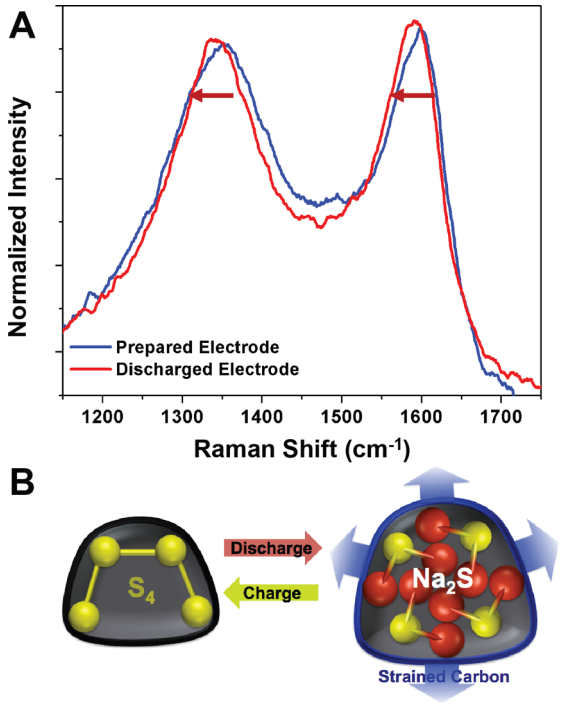

Figure 3. (A) Raman spectroscopy of an as-prepared slurry-cast electrode and fully discharged cathode. (B) Schematic representation of discharge mechanism inside a micropore that results in a strained carbon host.

combined with a stable anode−electrolyte interface enables a moderate energy density and long-term stability necessary for a practical stationary battery system. This infiltration method is significantly more scalable and less expensive compared to other methods that traditionally employ long (>20 h) melt techniques[14,15,25] to ensure pore infiltration or use high temperature (>300 °C) loadings for depolymerization of sulfur vapor.[26,30] Further experimental details on this technique are provided in the Supporting Information. Confinement in this electrode configuration is expected to promote only a transition from the largest S_4 molecules to Na_2S_2 and Na_2S sequentially, eliminating soluble products from the mechanism and preventing direct interaction between active sulfur and electrolyte.[7] This is because the pores are also too small to accommodate the solvent molecule (~0.7 nm in diameter).[36,37] In turn, the metal ion (only ~0.2 nm in diameter) must desolvate at the surface of the microporous host and transport independently to the sulfur, forming a quasi solid-state reaction at the cathode as opposed to the typical conversion battery configuration were ions transport through the electrolyte until reaching an active site before desolvating and readily converting.[14,15] Notably, whereas this technique specifically targets micropores due to the high free energy that drives capillary insertion of sulfur, higher loadings can be achieved by enhancing microporous volume or utilizing different strategies. Our previous work has achieved >80 wt % loading in sulfur cathodes where the confinement mechanism is not required.[35]

In order to verify uniform infiltration of sulfur, scanning transmission electron microscopy with energy dispersive spectroscopy (STEM EDS) elemental mapping was utilized. By visual inspection of the composite map revealing spatial distribution of carbon and sulfur (Figure 1E), the signature of both elements are uniform across the material. The individual element maps of carbon in blue (Figure 1F) and sulfur in

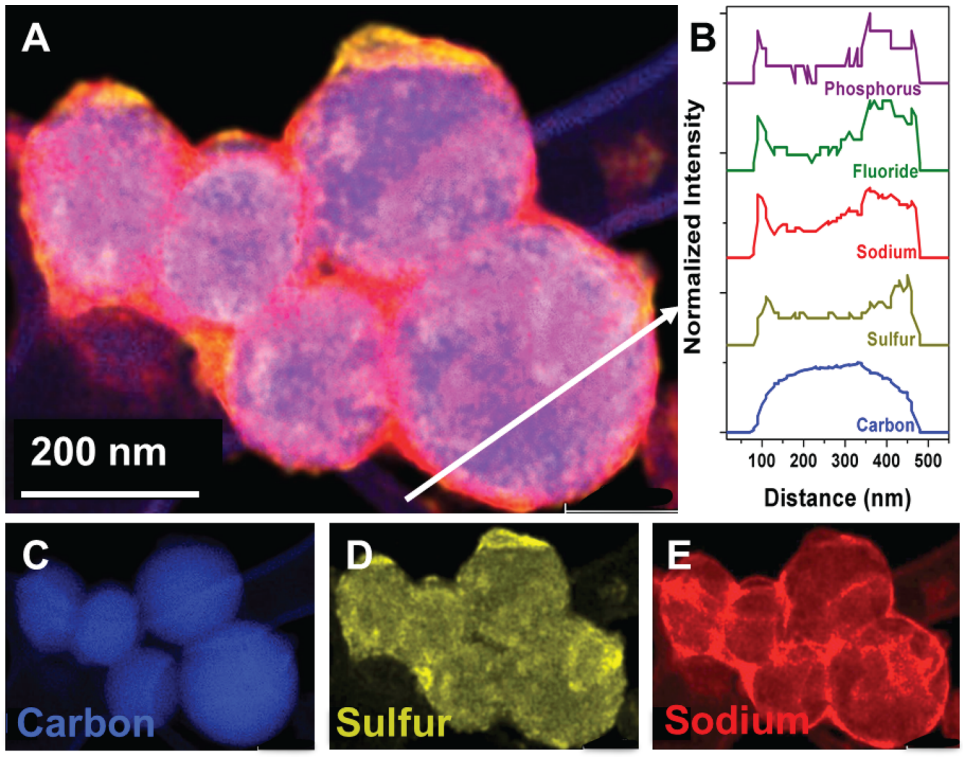

Figure 4. (A) STEM EDS composite map of fully discharged microporous carbon spheres with carbon (blue), sulfur (yellow), and sodium (red). (B) Linescan across the diameter of a microporous sphere with phosphorus (purple) and flouride (green) signatures arising from the electrolyte salt and carbon, sulfur, and sodium intensity plotted. (C−E) Individual element maps for carbon, sulfur, and sodium.

DOI: 10.1021/acs.nanolett.6b05172
Nano Lett. 2017, 17, 1863−1869

yellow (Figure 1G) show no differentiating features when in direct comparison and a uniform distribution of sulfur intensities (Figure 1G) across individual spheres, affirming the effectiveness of the isothermal vapor process in infiltrating the entirety of the spheres without build up at the surface. A line scan (Figure 1H) spanning the diameter of a sphere reveals a hill shaped response for both elements, indicative of the sphere geometry with highest signal at the middle and no signal at the exterior on each extremity of the line. Carbon and sulfur are detected throughout the sphere with minimal variation in intensity, emphasizing the complete and uniform penetration of sulfur through the material.

Raman spectroscopy was used to compare as prepared microporous carbon to sulfur infiltrated carbon and verify absence of S_8 molecules (Figure 1I). With 532 nm laser excitation the microporous carbon powder reveals defective carbon with characteristic G (sp^2 hybridized), and D (sp^3 hybridized) peaks at 1360 and 1592 cm^{-1}, respectively, and an I_D/I_G ratio of 0.91. This response along with the TEM image of the microporous morphology (Figure 1D) provides evidence of microporous pore size with disordered, partially graphitized carbon present. After sulfur infiltration, the spectra is observed to red shift by 17 cm^{-1} in the D peak, indicating both that sulfur that is primarily stored in defect sites (sp^3 hybridized carbon) where the spacing is largest and that an intimate interaction between sulfur and carbon defects exists. Additionally, no characteristic S_8 peaks were detected in the infiltrated material, indicating the sulfur is stored as smaller molecules without crystalline order and fully contained in the carbon material.

Upon verification of uniform sulfur infiltration and ideal microporous structure the powder is slurry-cast into cathodes and assembled into coin cells with sodium metal anodes. As opposed to using traditional organic carbonate electrolytes,[7] coin cells were assembled using $NaPF_6$ salts dissolved in tetraglyme as electrolyte. Building on previous studies that emphasize sodium anode stability during the reversible plating reaction in glymes,[32] this electrolyte was chosen to overcome the unstable SEI formation on Na metal anodes observed in carbonate-based electrolytes, which is critical to achieving good cycling performance. The discharge/charge behavior is first examined using cyclic voltammetry over the extended range of 0.5 to 2.7 V beginning with discharge from OCV of ∼1.7 V at scan rate of 50 μV/s (Figure 2A). Two peaks are detected on charge and discharge correlating to the two distinct transitions in the system to Na_2S_2 at ∼1.7 V and Na_2S at ∼0.9 V.[25] The second transition is prominent on the first discharge cycle and begins to match the intensity on first charge in subsequent cycles. These transitions are schematically illustrated on the voltammagram. An initial state and fully charged state of S_4 is depicted. However, there a range of molecule sizes from S_2−S_4 depending on the slight variation of pore size and shape throughout the material. S_4 is the largest molecule present, as confirmed by the presence of a two-step transition below the voltage where high order polysulfides form and geometric agreement with previous theoretical studies.[25] The S_4 requires full transition through both peaks on cycling. Smaller molecules will iterate through the appropriate transitions within the curve. Galvanostatic charge−discharge of the material was carried out at various rates over the voltage range of 0.8 to 2.6 V with representative profiles shown in Figure 2B. On first discharge at the slow rate of 0.1C (C = 1675 mA/g_S), the material reaches 91% of theoretical capacity and visual distinction between the two reaction plateaus, correlating to the peaks in Figure 2A, is present. Although the reaction voltages are less clear in the charge−discharge profiles, dQ/dV analysis (Figure S1) reveals peak locations through galvanostatic testing very similar to those observed in cyclic voltammetry. Additionally, similar to the observation in CV measurements, the transition to Na_2S recedes during cycling. This could be attributed to poor volume expansion accommodation in the material due to the native confinement in microporous volumes. Nonetheless, stable capacity and shapes of the CV and galvanostatic charge/discharge profiles suggest final discharge product of $Na_2S_{1.5}$ corresponding to ∼160% expansion is sustained by the material and its sodium storage capacity far surpasses elemental sulfur cathodes limited to the discharge product Na_2S_3[7] or half the sodium stored in our system. This stable discharge produces results and reversible capacity (700 mAh/g_S) and is capable of energy density of ∼180 Wh/kg when considering entire electrode mass (sulfur, microporous carbon, binder, carbon black, and ideal sodium anode). This metric emphasizes the competitive nature of this approach in relation to state-of-the-art commercial batteries after implementing extremely simplistic manufacturing methods.

Additionally, impressive rate capability exists as verified by reversible capacity of 370 mAh/g_S at high rates of 1C, which emphasizes over 50% retention of capacity at 10 times the rate. Notably, at all rates the Coulombic efficiency remains >98% (Figure 2C), which is quite remarkable compared to the extremely low Coulombic efficiencies ranging from 50 to 80% with elemental sulfur cathodes.[7] We attribute the high Coulombic efficiency to stable SEI formation at the sodium metal−electrolyte interface due to the glyme electrolyte as well as the quasi-solid state nature of the reaction where sodium ions transport through the resilient carbon material and react without contact with the glyme at the cathode.

Durability tests at 0.1C (Figure 2D) and 1C (Figure 2E) rates were also carried out. At 0.1C, a decay to ∼60% capacity retention in the first 20 cycles is followed by stable behavior (∼0.1% decay per cycle) for 230 subsequent cycles. The cathode tested at higher rates revealed similar behavior but after initial decay exhibited extremely stable capacity with 306 mAh/g_S delivered at cycle 1500. With respect to the entire mass of the electrode, the cathode delivers 87 mAh/g after 1500 cycles at 100% depth of discharge (DOD), which is an impressive mass specific performance especially with the moderate loading of 35 wt % active sulfur. This is amplified based on the premise that this material template is based on sugar, sulfur, and sodium and shows proof of concept for this approach to produce viable grid scale battery cathodes. In all cases, after the initial decay of reversible capacity, the Coulombic efficiency remained >98%.

In order to gain further insight into the behavior of the material during discharge, a cathode was cycled 20 times to reach the stable regime and then fully discharged cathode and examined using Raman spectroscopy and STEM EDS mapping. The electrode was retrieved from a discharged coin cell, sealed in an airtight window, and compared to an as-prepared electrode (Figure 3A). The discharged material revealed significant redshift of both the D and G carbon peaks of 12 and 14 cm^{-1}, respectively (Figure 3A). The final red shift of the D peak is >25 wavenumbers with combination of sulfur infiltration seen in Figure 1I and sodiation inside the carbon material (Figure 3A). The red shift of both peaks indicates strong tensile stress in the carbon as a result of the volume change as each sulfur attempts to store two sodium ions,

DOI: 10.1021/acs.nanolett.6b05172
Nano Lett. 2017, 17, 1863−1869

theoretically leading to a 260% volume expansion (Figure 2B). In order to support the observation of tensile force of the material as a result of sodium-induced volume expansion, STEM EDS was used to verify uniform confinement of sodium throughout the material. The composite map in Figure 4A shows the distribution of sodium, sulfur, and carbon in a cluster of discharged spheres. Line scans taken across the largest sphere shows sodium distributed throughout with a response revealing the combined presence of the electrolyte (fluoride and phosphorus) and sulfur, verifying its presence and reactivity with sulfur. The X-ray spectrum is provided in Figure S3. The individual element maps with carbon mapped blue (Figure 4C), sulfur mapped yellow (Figure 4D) and sodium mapped red (Figure 4E) further emphasize the uniform loading of sulfur throughout the carbon and the complete penetration of sodium on the interior of the microporous carbon with some apparent dried electrolyte across the surface. This ex situ characterization helps to verify the ability of sodium to fully access the microporous spheres (TEM), as well as significant tensile stress in the system as the material accommodates sodium ions on discharge (Raman spectroscopy).

Overall, our work demonstrates the capability to produce a room-temperature sodium sulfur battery based on combined electrode components of sodium, sulfur, and processed table sugar. Compared to other approaches, the high Coulombic efficiency, microporous confinement of discharge products, and electrolyte that leads to a stable SEI on the sodium anode gives rise to high performance with stable cycling over 1500 cycles at high rates of 1C where a capacity >300 mAh/g_S is maintained compared to reversible capacities at slow rates of 0.1C where >700 mAh/g_S is measured. This work presents an attractive platform for future battery design, both for a cheap alternative to lithium-ion batteries where the competitive cathode gravimetric capacity in sugar derived sulfur cathodes rivals that of cobalt-containing cathodes in lithium-ion batteries, and a practical stationary grid storage system where excellent rate performance, cyclability, and simplicity of materials leads to promise for lifetime cost per kWh that can be significantly lower than conventional power generation.

■ ASSOCIATED CONTENT

Supporting Information

The Supporting Information is available free of charge on the ACS Publications website at DOI: 10.1021/acs.nanolett.6b05172.

Experimental details, comparison of confinement strategy for lithium and sodium sulfur batteries, comparison of sodium sulfur batteries with and without confinement, and X-ray spectra of both STEM EDS maps (PDF)

■ AUTHOR INFORMATION

Corresponding Author

*E-mail: cary.l.pint@vanderbilt.edu.

ORCID

Nitin Muralidharan: 0000-0001-6042-5295

Cary L. Pint: 0000-0003-4700-0852

Notes

The authors declare no competing financial interest.

■ ACKNOWLEDGMENTS

The authors acknowledge Keith Share, Andrew Westover, and Mengya Li for helpful discussions. This work was supported in part by NSF Grant CMMI 1400424, A.C. and A.D. were supported by NSF graduate fellowships under Grant 1445197, and R.C. acknowledges support from a graduate fellowship provided by the Vanderbilt Institute of Nanoscale Science and Technology.

■ REFERENCES

(1) Lu, X. C.; Xia, G. G.; Lemmon, J. P.; Yang, Z. G. *J. Power Sources* **2010**, *195*, 2431−2442.

(2) Dunn, B.; Kamath, H.; Tarascon, J. M. *Science* **2011**, *334*, 928−935.

(3) Larcher, D.; Tarascon, J. M. *Nat. Chem.* **2014**, *7*, 19−29.

(4) Manthiram, A.; Yu, X. W. *Small* **2015**, *11*, 2108−2114.

(5) Scheers, J.; Fantini, S.; Johansson, P. *J. Power Sources* **2014**, *255*, 204−218.

(6) Seh, Z. W.; Sun, Y. M.; Zhang, Q. F.; Cui, Y. *Chem. Soc. Rev.* **2016**, *45*, 5605−5634.

(7) Adelhelm, P.; Hartmann, P.; Bender, C. L.; Busche, M.; Eufinger, C.; Janek, J. *Beilstein J. Nanotechnol.* **2015**, *6*, 1016−1055.

(8) Kohl, M.; Borrmann, F.; Althues, H.; Kaskel, S. *Adv. Energy Mater.* **2016**, *6*, 201502185.

(9) Yu, X. W.; Manthiram, A. *Adv. Energy Mater.* **2015**, *5*, 201500350.

(10) Yu, X. W.; Manthiram, A. *Chem. Mater.* **2016**, *28*, 896−905.

(11) Yu, X. W.; Manthiram, A. *Chem. - Eur. J.* **2015**, *21*, 4233−4237.

(12) Xu, Y. H.; Wen, Y.; Zhu, Y. J.; Gaskell, K.; Cychosz, K. A.; Eichhorn, B.; Xu, K.; Wang, C. S. *Adv. Funct. Mater.* **2015**, *25*, 4312−4320.

(13) Niu, S. Z.; Zhou, G. M.; Lv, W.; Shi, H. F.; Luo, C.; He, Y. B.; Li, B. H.; Yang, Q. H.; Kang, F. Y. *Carbon* **2016**, *109*, 1−6.

(14) Zhang, B.; Qin, X.; Li, G. R.; Gao, X. P. *Energy Environ. Sci.* **2010**, *3*, 1531−1537.

(15) Xin, S.; Gu, L.; Zhao, N. H.; Yin, Y. X.; Zhou, L. J.; Guo, Y. G.; Wan, L. J. *J. Am. Chem. Soc.* **2012**, *134*, 18510−18513.

(16) Helen, M.; Reddy, M. A.; Diemant, T.; Golla-Schindler, U.; Behm, R. J.; Kaiser, U.; Fichtner, M. *Sci. Rep.* **2015**, *5*, 12146.

(17) Yu, X. W.; Manthiram, A. *J. Phys. Chem. C* **2014**, *118*, 22952−22959.

(18) Yu, X. W.; Manthiram, A. *J. Phys. Chem. Lett.* **2014**, *5*, 1943−1947.

(19) Ryu, H.; Kim, T.; Kim, K.; Ahn, J. H.; Nam, T.; Wang, G.; Ahn, H. J. *J. Power Sources* **2011**, *196*, 5186−5190.

(20) Kim, I.; Park, J. Y.; Kim, C.; Park, J. W.; Ahn, J. P.; Ahn, J. H.; Kim, K. W.; Ahn, H. J. *J. Electrochem. Soc.* **2016**, *163*, A611−A616.

(21) Hwang, T. H.; Jung, D. S.; Kim, J. S.; Kim, B. G.; Choi, J. W. *Nano Lett.* **2013**, *13*, 4532−4538.

(22) Bauer, I.; Kohl, M.; Althues, H.; Kaskel, S. *Chem. Commun.* **2014**, *50*, 3208−3210.

(23) Wenzel, S.; Metelmann, H.; Raiss, C.; Durr, A. K.; Janek, J.; Adelhelm, P. *J. Power Sources* **2013**, *243*, 758−765.

(24) Jeong, G.; Kim, H.; Lee, H. S.; Han, Y. K.; Park, J. H.; Jeon, J. H.; Song, J.; Lee, K.; Yim, T.; Kim, K. J.; Lee, H.; Kim, Y. J.; Sohn, H. J. *Sci. Rep.* **2015**, *5*, 12827.

(25) Xin, S.; Yin, Y. X.; Guo, Y. G.; Wan, L. J. *Adv. Mater.* **2014**, *26*, 1261−1265.

(26) Wang, J. L.; Yang, J.; Nuli, Y.; Holze, R. *Electrochem. Commun.* **2007**, *9*, 31−34.

(27) Chen, Y. M.; Liang, W. F.; Li, S.; Zou, F.; Bhaway, S. M.; Qiang, Z.; Gao, M.; Vogt, B. D.; Zhu, Y. *J. Mater. Chem. A* **2016**, *4*, 12471−12478.

(28) Lee, D. J.; Park, J. W.; Hasa, I.; Sun, Y. K.; Scrosati, B.; Hassoun, J. *J. Mater. Chem. A* **2013**, *1*, 5256−5261.

(29) Kim, I.; Kim, C. H.; Choi, S. H.; Ahn, J. P.; Ahn, J. H.; Kim, K. W.; Cairns, E. J.; Ahn, H. J. *J. Power Sources* **2016**, *307*, 31−37.

(30) Fan, L.; Ma, R. F.; Yang, Y. H.; Chen, S. H.; Lu, B. A. *Nano Energy* **2016**, *28*, 304−310.

DOI: 10.1021/acs.nanolett.6b05172
Nano Lett. 2017, 17, 1863−1869

(31) Ye, X. M.; Ma, J.; Hu, Y. S.; Wei, H. Y.; Ye, F. F. *J. Mater. Chem. A* **2016**, *4*, 775−780.
(32) Seh, Z. W.; Sun, J.; Sun, Y. M.; Cui, Y. *ACS Cent. Sci.* **2015**, *1*, 449−455.
(33) Scherdel, C.; Reichenauer, G. *Carbon* **2009**, *47*, 1102−1111.
(34) Guo, P. Z.; Gu, Y.; Lei, Z. B.; Cui, Y. Q.; Zhao, X. S. *Microporous Mesoporous Mater.* **2012**, *156*, 176−180.
(35) Oakes, L.; Carter, R.; Pint, C. L. *Nanoscale* **2016**, *8*, 19368−19375.
(36) Li, Z.; Yuan, L. X.; Yi, Z. Q.; Sun, Y. M.; Liu, Y.; Jiang, Y.; Shen, Y.; Xin, Y.; Zhang, Z. L.; Huang, Y. H. *Adv. Energy Mater.* **2014**, *4*, 201301473.
(37) Kim, H.; Hong, J.; Yoon, G.; Kim, H.; Park, K. Y.; Park, M. S.; Yoon, W. S.; Kang, K. *Energy Environ. Sci.* **2015**, *8*, 2963−2969.

DOI: 10.1021/acs.nanolett.6b05172
Nano Lett. 2017, 17, 1863−1869